Electronic Supplementary Material (ESI) for Journal of Materials Chemistry A.

Supporting Information

Formation of a photoactive quasi-2D formamidinium lead iodide perovskite in water

Atanu Jana,‡ Qiankai Ba,‡ Arun S. Nissimagoudar, and Kwang S. Kim*

Center for Superfunctional Materials, Department of Chemistry, School of Natural Science, Ulsan National Institute of Science and Technology (UNIST), 50 Unist-gil, Ulsan 44919, South Korea.

E-mail: kimks@unist.ac.kr

‡These authors contributed equally to the work.

Experimental Section

Materials

Lead(II) carbonate basic [$PbCO_3)_2.Pb(OH)_2$, 325 mesh], formamidinium acetate ($HN{=}CHNH_2.CH_3COOH$, 99%), octylamine (OAm, 99%), hydroiodic acid (HI, 57 wt. % in H_2O, distilled, stabilized, 99.95%), ethyl acetate ($CH_3COOCH_2CH_3$, anhydrous, 99.8%) were purchased from sigma-Aldrich.

Synthesis of δ-phase $FAPbI_3$:

Basic lead carbonate (0.5 mmol, 0.388 gm) and formamidinium acetate (1.5 mmol, 0.156 gm) were added in HI (2 ml) and immediately yellow colored precipitate appeared. To achieve the full conversion, the precipitate was sonicated for 5 minutes and then washed with ethyl acetate (15 ml). The yellow precipitate was dried in oven at 60 °C.

Synthesis of α-phase $FAPbI_3$ NCs:

In a typical synthesis of **1**, basic lead carbonate (0.5 mmol, 0.388 gm) and formamidinium acetate (1.5 mmol, 0.156 gm) were added in HI (2 ml) and immediately yellow colored precipitate appeared. To achieve the full conversion, the precipitate was sonicated for 5 minutes. In a separate vial (2 ml) octylamine (3 mmol, 500 µl) was taken and then HI (3 mmol, 576 µl) was added. The light yellow solution was added to the 20 ml vial and sonicated for 5 minutes to achieve the full conversion. At this stage, it became a high viscous solid which was a deep red color. The product was washed with ethyl acetate (10 ml) and dried at 60 °C for overnight.

For the preparation of compounds **2**, **3** and **4**, we used different amounts of octylamine (OAm) such as 50 µl, 300 µl, and 800 µl, respectively, and same mole ratios of HI as that of OAm in each case. The amounts of basic lead carbonate (0.5 mmol, 0.388 gm) and formamidinium acetate (1.5 mmol, 0.156 gm) were the same for syntheses of **2**, **3**, and **4**.

Characterization Methods

The powder X-ray diffraction was performed on D/MAX2500V/PC diffractometer, Rigaku using Cu-rotating anode x-ray.

X-ray photoelectron spectra (XPS) were collected using K-alpha model, ThermoFisher. During the measurement, the Bragg's diffraction angle (2θ) range was set to 10-50° and scan rate was 2°/ minute.

Scanning electron microscopy (SEM) images were captured in SU8220 Cold FE-SEM, Hitach High-Technologies under an acceleration voltage of 10 kV. Energy Dispersive X-Ray Spectroscopy (EDS) was done to characterize the elements of all the samples.

X-ray photoelectron spectroscopy (XPS) was performed in K-alpha (ThermoFisher) to analyze the chemical compositions.

The optical diffuse reflectance spectra were collected using a Cary 5000 UV-Vis-NIR Spectrophotometer (Agilent) with an integrated sphere in diffuse-reflectance mode and then converted to UV-Vis diffuse reflectance spectra [F(R) vs wavelength (nm)] using Kubelka-Munk function, F(R).

All the photoluminescence (PL) spectra were taken in Cary Eclipse fluorometer, (Varian) in solid-state.

Fourier-transform infrared spectra (FTIR) were taken in FTIR (670-IR, Varian) with attenuated total reflection detector.

The photoluminescence single-particle imaging was carried out in LSM 780 NLO (maker: Carl Zeiss). Powder samples are spread in glass. The focus of the samples were adjusted mechanically using 10 × air and 100 × oil objective lenses. The laser used in the experiment was 405 nm. The detection range was 410-700 nm (8.9 nm). We used a GaAsP PMT detector (32 channels) for the measurements.

Thermogravimetric analysis (TGA) was performed using Q500 model, TA. The heating rate was maintained at 10^0/ minute.

Density functional theory calculations.

All our first-principles density functional theory (DFT) calculations were performed using the plane-wave formalism as implemented in the Vienna ab initio simulation package (VASP).[1,2] The exchange and correlation part of the total energy is approximated by the generalized gradient approximation (GGA) using the Perdew–Burke– Ernzerhof (PBE)[3] type of functional. The core–valence interaction is described by the projector-augmented wave method. We have also considered the DFT-D3 van der Waals correction method of Graimme[4] to introduce dispersive interactions within the system. Plane wave functions were expanded with an energy cutoff of 500 eV and Brillouin zone sampled using an 8x8x8 gamma centered k-mesh. Structural relaxation was performed by fixing lattice parameter, a = 6.3620 Å[5] for α- $FAPbI_3$ ($Pm\bar{3}m$) and a = 8.6603 Å, c = 7.902 Å[6] for δ-$FAPbI_3$ ($P6_3mc$) and all atoms were fully relaxed using the conjugate-gradient method until the absolute values of the Hellman–Feynman forces were converged to within 0.005 eV/Å. In the case of slab model, we chose 4×4×2 gamma centered k-mesh and vacuum thickness 15 Å to avoid spurious interactions between the slab and its periodic images.

Table S1. Various synthetic conditions, precursor salts and solvents for synthesis of α-$FAPbI_3$ NCs

Serial number	**α-phase $FAPbI_3$ NCs**		
	Temperature	**Precursor salts**	**Solvents/Capping ligands**
A[7]	40–60 °C	FA-oleate, Pb-oleate	1-octadecene, oleic acid, oleylamine
B[8]	80 °C	FA-oleate, Pb-oleate	1-octadecene, oleic acid, oleylamine
C[9]	Room temperature (RT)	Formamidinium iodide (FAI), PbI_2	N,N-dimethylformamide (DMF), oleic acid, oleylamine
D[10]	125 °C and 75–95 °C	Lead acetate trihydrate, formamidinium acetate	1-octadecene, oleic acid, oleylamine, benzoyl iodide
E[11]	120 °C and 80 °C	FA-oleate, PbI_2	1-octadecene, oleic acid, oleylamine
F[12]	60 ˚C and 100 ˚C	FAI and PbI_2	γ-butyrolactone (GBL),
G[13]	70 ˚C and RT	PbI_2-DMSO, FAI	DMF, oleic acid, oleylamine
H (Current work)	RT (20 ˚C)	$(PbCO_3)_2.Pb(OH)_2$, formamidinium acetate	Aqueous HI, octylamine

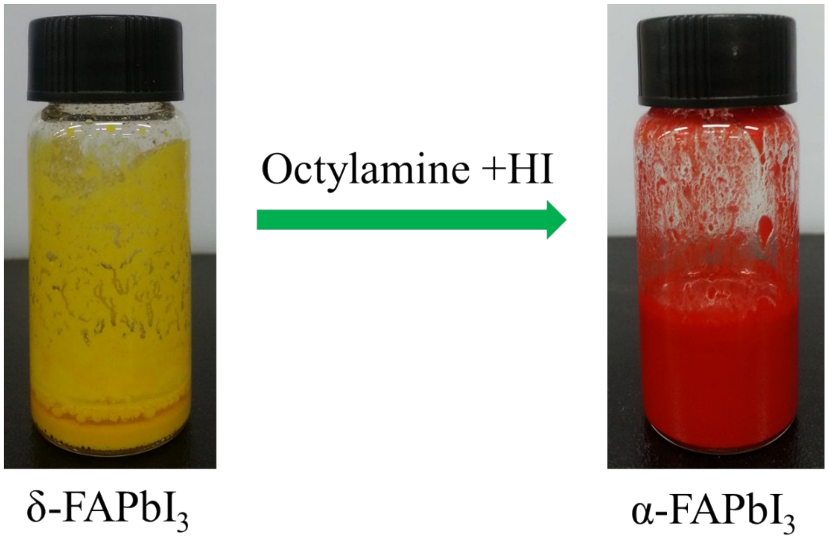

Fig. S1. Photographs during synthesis. (a) δ-$FAPbI_3$ and (b) α-$FAPbI_3$ (**1**).

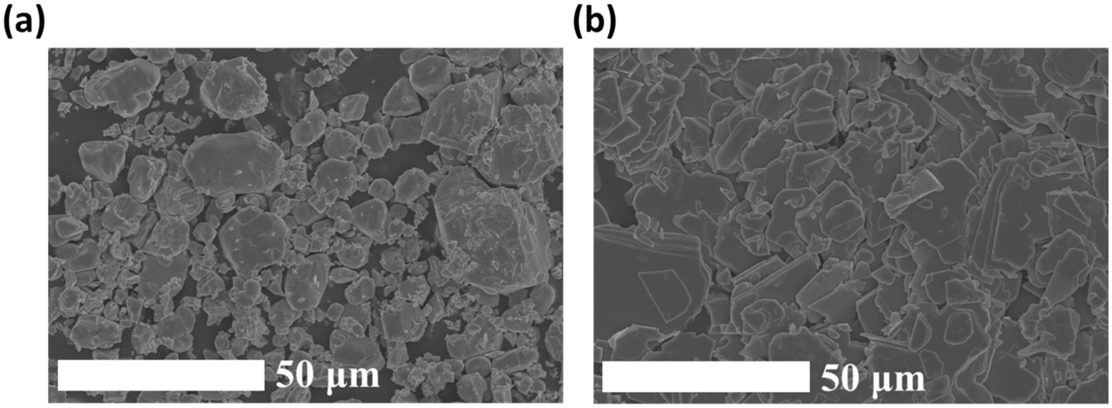

Fig. S2. SEM images. (a) δ-$FAPbI_3$ and (b) α-$FAPbI_3$ NCs (**1**).

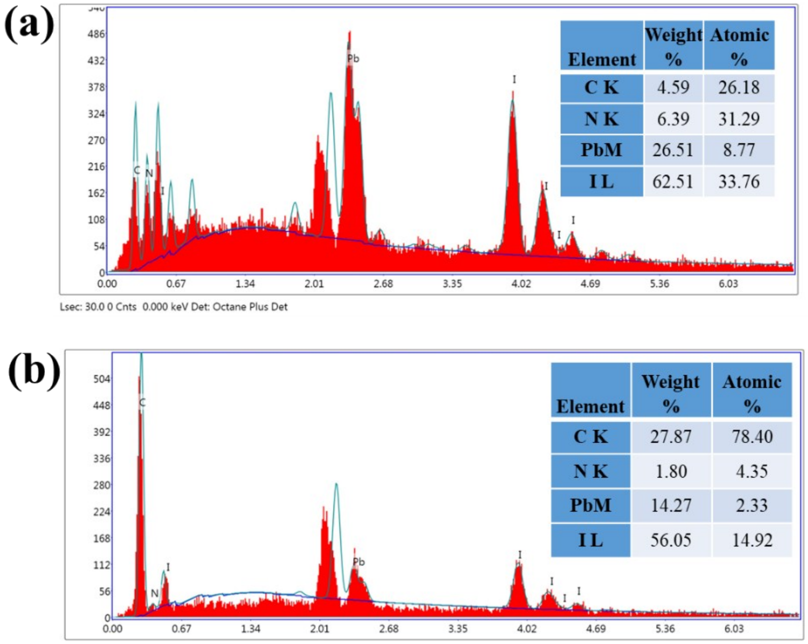

(a)

Element	Weight %	Atomic %
C K	4.59	26.18
N K	6.39	31.29
PbM	26.51	8.77
I L	62.51	33.76

(b)

Element	Weight %	Atomic %
C K	27.87	78.40
N K	1.80	4.35
PbM	14.27	2.33
I L	56.05	14.92

Fig. S3. SEM-EDS. (a) δ-$FAPbI_3$ and (b) α-$FAPbI_3$ (**1**).

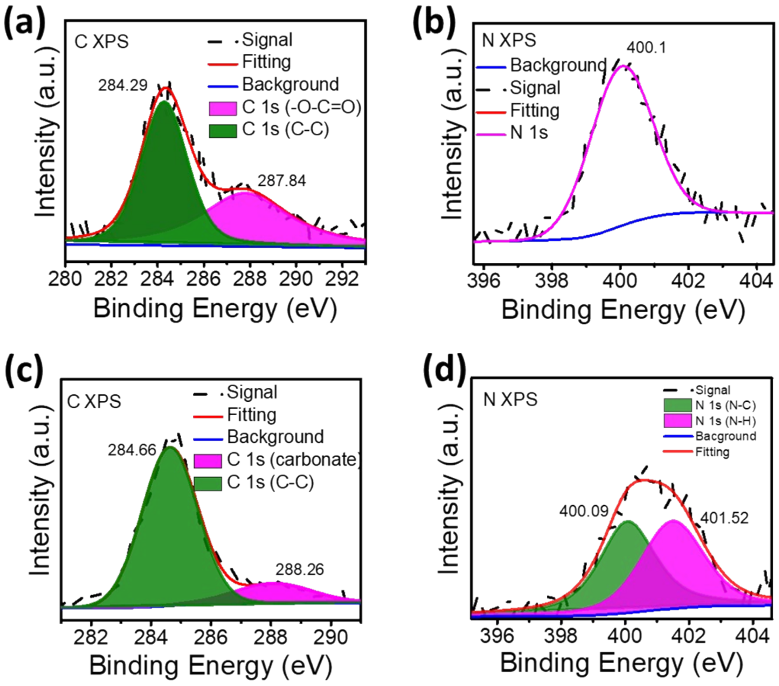

Fig. S4. XPS spectra. (a, b) δ-$FAPbI_3$ and (c, d) α-$FAPbI_3$ (**1**).

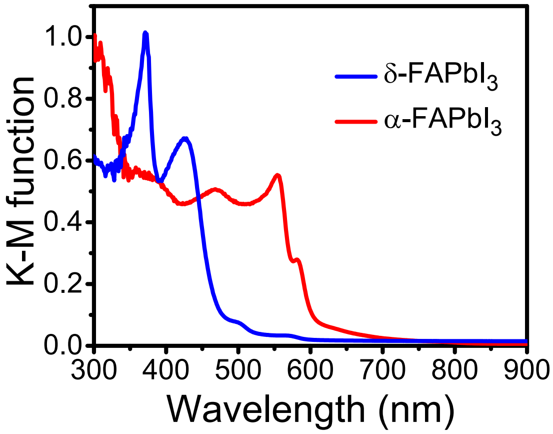

Fig. S5. UV−vis diffuse reflectance spectra of δ-$FAPbI_3$ and α-$FAPbI_3$ NCs (**1**). K-M means Kubelka−Munk function.

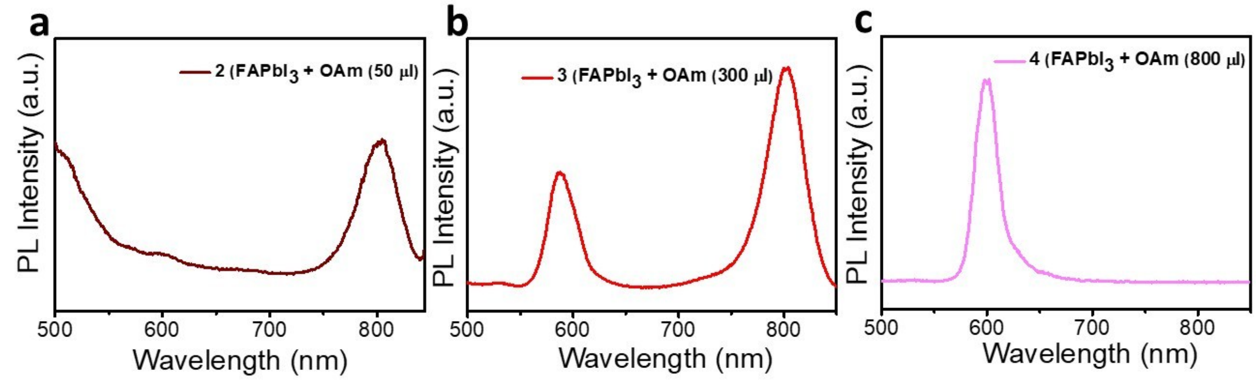

Fig. S6. Emission spectra of **2**, **3,** and **4**.

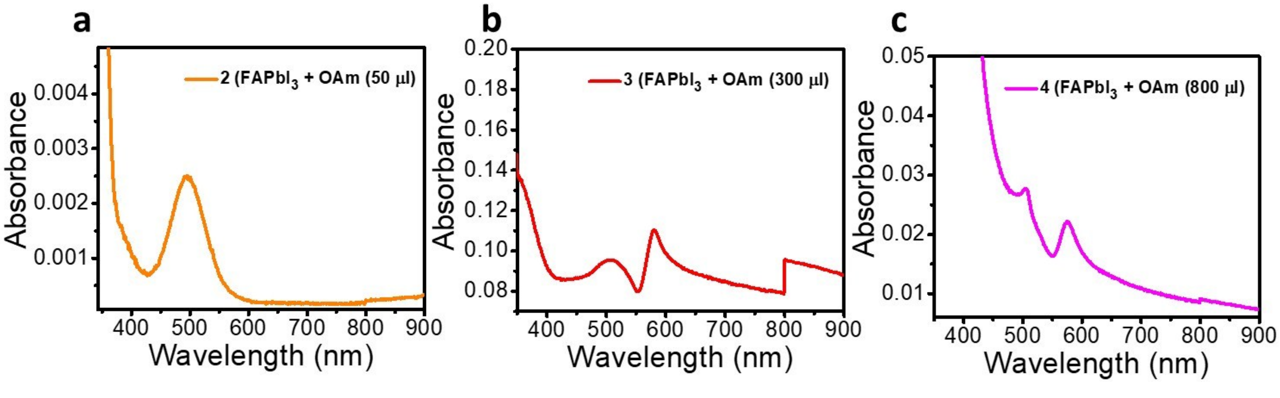

Fig. S7. Absorbance spectra of **2**, **3,** and **4**.

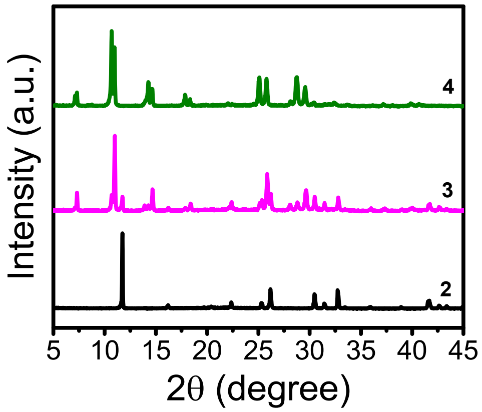

Fig. S8. PXRD of **2**, **3,** and **4**.

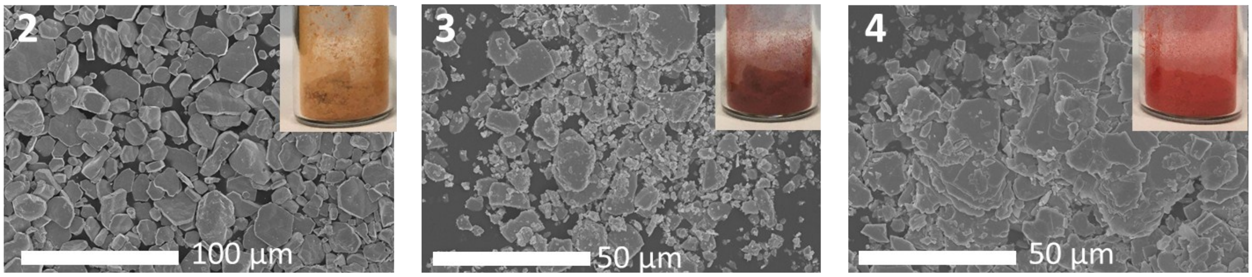

Fig. S9. SEM images of **2**, **3,** and **4** and their respective images (inset) of powder samples under visible light.

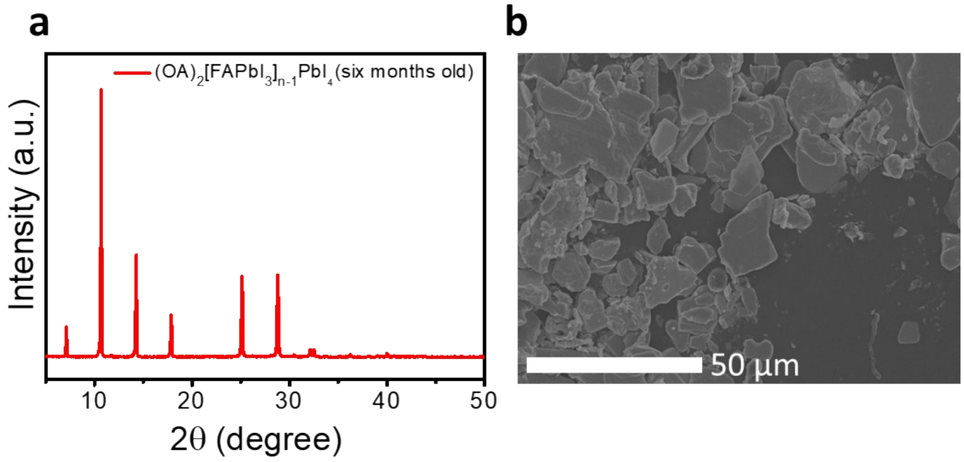

Fig. S10. (a) PXRD and (b) SEM image of **1** taken after six months. The crystal structure and morphology are same as the initial samples and this confirms the stability of **1**.

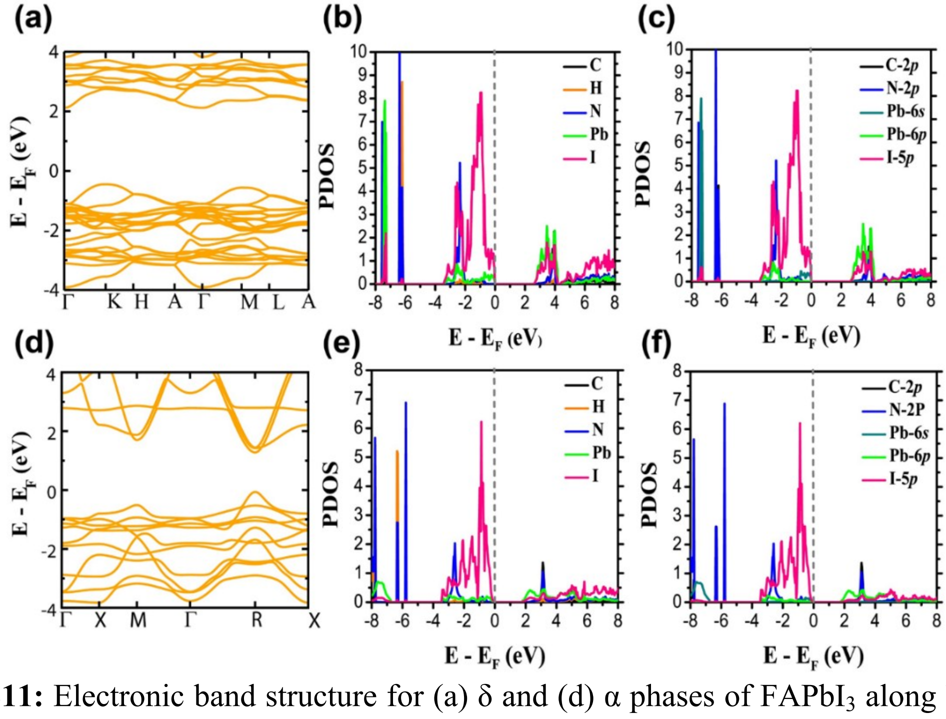

Fig. S11: Electronic band structure for (a) δ and (d) α phases of $FAPbI_3$ along high symmetry directions. Projected density of states for (b) δ phase and (e) α phases of $FAPbI_3$ per element in unit cell, and partial orbits of C, N, Pb and I for (c) δ phase and (f) α phases of $FAPbI_3$.

For the δ phase the main contribution to valence band is from I 5*p* states, and a smaller contribution from Pb 6*s* 6*p* states. Contribution to conduction band is dominated by both I 5*p* and 6*p* states along with smaller contributions, from C 2*p* and N 2*p* states. For α phase, the contribution to valence band is dominated from I 5*p* states with smaller contribution from Pb 6s and N 2p states. Conduction band of α phase is dominated by I 5*p*, Pb 6*p*, C 2*p* and N 2*p* states. These analyses indicate that in both phases the organic cation (FA^+) has considerable influence in conduction band in addition to significant contribution from metallic cation (Pb) and the halide anion (I), which in turn enhance the electronic properties. From the charge density associated with valence band maximum (VBM) and conduction band minimum (CBM) for δ and α phases of $FAPbI_3$, one finds that for the δ case VBM is derived from the I 5*p* interaction and CBM is derived from the Pb 6*p* and I 5*p* interactions. For the case of α phase contribution to VBM comes from the I 5*p* interaction while CBM is derived from the I 5*p*, C 2*p* and N 2*p* interactions.

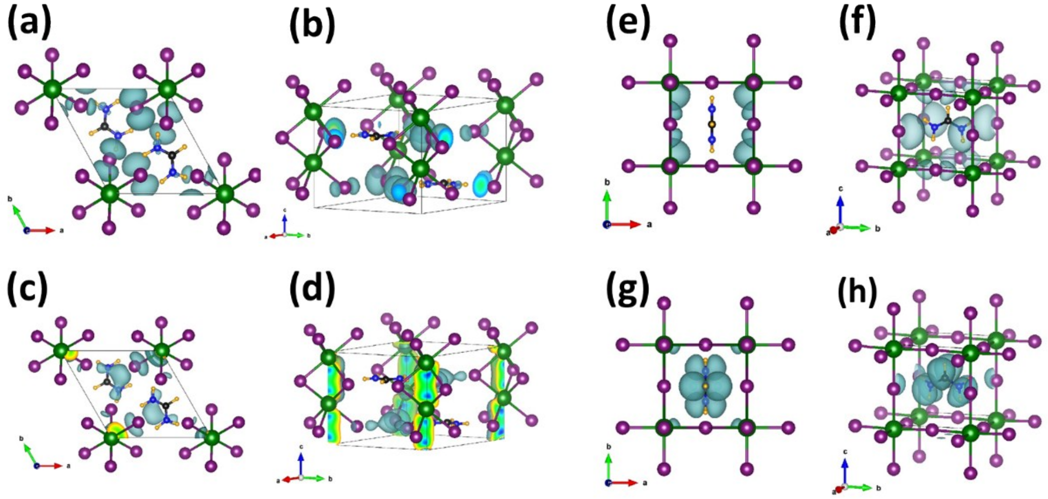

Fig. S12: Charge density corresponding to states near VBM [(a, e) <001> view, (b, f) <100> view] and near CBM [(c, g) <001> view and (d, h) <100> view] for δ and α phases, respectively. Iso-surface value is 3×10^{-3} eV/ Å^3.

References

1 G. Kresse and J. Furthmüller, *Physical Review B*, 1996, **54**, 11169–11186.

2 G. Kresse and J. Furthmüller, *Computational Materials Science*, 1996, **6**, 15–50.

3 J. P. Perdew, K. Burke and M. Ernzerhof, *Physical Review Letters*, 1996, **77**, 3865–3868.

4 S. GRIMME, *Journal of Computational Chemistry*, 2009, **30**, 1174–1178.

5 M. T. Weller, O. J. Weber, J. M. Frost and A. Walsh, *The Journal of Physical Chemistry Letters*, 2015, **6**, 3209–3212.

6 C. C. Stoumpos, C. D. Malliakas and M. G. Kanatzidis, *Inorganic Chemistry*, 2013, **52**, 9019–9038.

7 R. M. MacEiczyk, K. Dümbgen, I. Lignos, L. Protesescu, M. V. Kovalenko and A. J. Demello, *Chemistry of Materials*, 2017, **29**, 8433–8439.

8 L. Protesescu, S. Yakunin, S. Kumar, J. Bär, F. Bertolotti, N. Masciocchi, A. Guagliardi, M. Grotevent, I. Shorubalko, M. I. Bodnarchuk, C. J. Shih and M. V. Kovalenko, *ACS Nano*, 2017, **11**, 3119–3134.

9 I. Levchuk, A. Osvet, X. Tang, M. Brandl, J. D. Perea, F. Hoegl, G. J. Matt, R. Hock, M. Batentschuk and C. J. Brabec, *Nano Letters*, 2017, **17**, 2765–2770.

10 M. Imran, V. Caligiuri, M. Wang, L. Goldoni, M. Prato, R. Krahne, L. De Trizio and L. Manna, *Journal of the American Chemical Society*, 2018, **140**, 2656–2664.

11 J. Xue, J.-W. Lee, Z. Dai, R. Wang, S. Nuryyeva, M. E. Liao, S.-Y. Chang, L. Meng, D. Meng, P. Sun, O. Lin, M. S. Goorsky and Y. Yang, *Joule*, 2018, **2**, 1866–1878.

12 A. M. Askar, A. Karmakar, G. M. Bernard, M. Ha, V. V. Terskikh, B. D. Wiltshire, S.

Patel, J. Fleet, K. Shankar and V. K. Michaelis, *Journal of Physical Chemistry Letters*, 2018, **9**, 2671–2677.

13 D. N. Minh, J. Kim, J. Hyon, J. H. Sim, H. H. Sowlih, C. Seo, J. Nam, S. Eom, S. Suk, S. Lee, E. Kim and Y. Kang, *Chemistry of Materials*, 2017, **29**, 5713–5719.